出國報告(出國類別:學術研討會)

赴日本參加
The 16th International Symposium on Flow Visualization (ISFV 2014)
返國報告

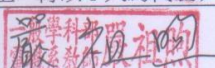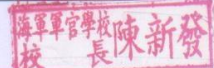服 務 機 關 ：海軍軍官學校
姓 名 職 稱 ：嚴祖煦副教授
派 赴 國 家 ：日本
報 告 日 期 ：103 年 6 月 25 日
出 國 時 間 ：103 年 6 月 24 日－30 日

出國報告審核表

出國報告名稱：赴日本參加 ISFU 2014返國報告

出國人姓名 （2人以上，以1人為代表）	職稱	服務單位
嚴祖煦	教師	海軍軍官學校

出國類別	☐考察 ☐進修 ☐研究 ☐實習 ☑其他 參加國際研討會（例如國際會議、國際比賽、業務接洽等）

出國期間：103.6.24 － 103.6.30　　報告繳交日期：103.7.3

出國人員 自我檢核	計畫主辦 機關審核	審　核　項　目
☑	☑	1.依限繳交出國報告
☑	☑	2.格式完整（本文必須具備「目的」、「過程」、「心得及建議事項」）
☑	☑	3.無抄襲相關資料
☑	☑	4.內容充實完備
☑	☑	5.建議具參考價值
☐	☐	6.送本機關參考或研辦
☐	☐	7.送上級機關參考
☐	☐	8.退回補正，原因：
☐	☐	（1）不符原核定出國計畫
☐	☐	（2）以外文撰寫或僅以所蒐集外文資料為內容
☐	☐	（3）內容空洞簡略或未涵蓋規定要項
☐	☐	（4）抄襲相關資料之全部或部分內容
☐	☐	（5）引用其他資料未註明資料來源
☐	☐	（6）電子檔案未依格式辦理
☐	☐	（7）未於資訊網登錄提要資料及傳送出國報告電子檔
☑	☑	9.本報告除上傳至出國報告資訊網外，將採行之公開發表：
☐	☐	（1）辦理本機關出國報告座談會（說明會），與同仁進行知識分享。
☐	☐	（2）於本機關業務會報提出報告
☑	☑	（3）其他 與系上同仁進行知識分享
☐	☐	10.其他處理意見及方式：

出國人簽章（2人以上，得以1人為代表）	計畫主辦機關審核人	一級單位主管簽章	機關首長或其授權人員簽章
嚴祖煦		林俊凱 代	陳新發 校長

說明：

一、各機關可依需要自行增列審核項目內容，出國報告審核完畢本表請自行保存。

二、審核作業應儘速完成，以不影響出國人員上傳出國報告至「公務出國報告資訊網」為原則。

1

摘要

　　計畫主持人於 2014 年 6 月 24 日清晨由高雄小港機場出關後，轉機桃園國際機場前往日本琉球(Okinawa, Japan)，於中午到達目的地後準備提報資料。6 月 25 下午發表論文，題目為 Effects of wettability on gas-water flow over the roughness nanochannels。內容是報告為水流通過含有氣泡的奈米流道時，固液介面的潤濕性、表面粗糙度以及表面微氣泡對於固液介面所產生的影響。並且探討由這些影響，進一步造成的介面與流場變化。報告中側重現象背後之物理機制。報告後多人發問與發表建言，討論熱烈。

　　會議期間，主持人除了吸取流體研究的新進成果外，亦與一些研究學者討論流場的模擬、量測技術以及流場可視化在產業上應用的知識與技術。獲益良多。

目次

出席國際會議心得報告

一、目的：

　　與國際學者討論交流有關流體在不同介面與環境下的計算、量測與應用，並發表個人論文。

二、會議概況：

　　國際流場可視化論壇（ISFV）每兩年舉辦一次。此次為第 15 屆，於 2014 年 6 月 24 日至 29 日在日本沖繩之 Okinawa Convention Center 舉行。研討內容偏重流場可視化、量測、相關數據資料的成相技術以及現象觀察與物理機制探討。本次大會邀請了各國頂尖之研究學者提出專題報告，參加的論文超過三百篇。為了提升流場可視化研究的重要性，大會除了在 PIV/PTV 量測外，開闢了數個不同領域的論文場次，包含有微奈米流、二相流、高速流動以及數值可視化等場次。大會並邀請一系列的專題演講，主要課題為如何運用先進之技術與創新的原理來突破先前難以觀察與量測的流場。這些極微小、多相或高速下的流場探討，提升了各領域應用上的多種可能。此外，流場觀測的歷史與藝術、能源領域與生醫科技的應用等場次，擴展了本次會議的視野與產業應用上的發展潛力。

三、過程與心得：

　　計畫主持人參與會議經過，如下所述：

　　計畫主持人於 2013 年 6 月 24 日凌晨由高雄小港機場出關後，轉桃園國際機場前往日本琉球(Okinawa, Japan)，於上午到達目的地後即準備次日之發表資料。

　　個人於 6 月 25 日下午發表論文，題目為 Effects of wettability on gas-water flow over the roughness nanochannels。主要內容為探討固液介面的潤濕性以及表面粗糙度，對於表面奈米尺度氣泡的形成以及外型影響，進而影響流體（包含水分子以及氣體分子）通過流道時所產生的滑移現象。報告中側重流場的密度分布、介面勢能分布以及傳輸性質（包含擴散係數、水分子旋轉運動的自相關函數）的計算，並且據以探討其介面現象與物理機制。報告後多人發問與發表建言，討論熱烈。其中有學者對於論文提問有關流道尺度縮小所可能的應用方向、流體傳輸性質所代表的物理意義；另有學者則是詢問可能的實驗設計以及與模擬結果的比對驗證。顯示此一領域的國際學者在研究上是理論與實驗技術並重的。

　　大會於 25 日至 27 日安排了一系列的專題演講，其中包含了愛荷華州立大學的 Hui Hu

教授以先進流場診斷技術量測流場的研究結果。德國 Delft 工業大學的 Poelma 教授發表了量測動態水滴接觸角的量測研究。此外，韓國 Pusan 大學的 Kyung chun Kim 教授介紹了反向電潤濕(REOW)發電的概念。並且利用此一概念展示了實際發電的成果。這些研究與個人的研究相當有關連，也激發了個人在相關研究上的靈感。

在 25 日的專題演講中，愛荷華州立大學的 Hui Hu 教授介紹以 DFD(Digital Fringe Projection)系統來達到非侵入式動態液滴與液膜的即時測量。其團隊所使用的 DFD 技術，原理為基於三角測量法的光投影技術。由投影機投影出的線條樣態，並藉由比對基準線與物體的線條樣態相變化，推算出物體的三維外型。其研究針對機翼結冰、風力發電葉片在結冰狀態下，水液滴在結冰表面的行為。尤其瞭解液滴在風驅動下，所產生的外型改變、前後沿接觸線的前進速度，尤其以液滴的跳躍行為以及水滴在結冰表面的熱傳現象等課題。在德國 Delft 工業大學的 Poelma 教授的專題演講中，其團隊針對沈浸式平版印刷(Immersion Lithography)法中，所可能遭遇液滴運動所造成的外型與穩定度改變，做實驗上的研究。與 Hui Hu 教授不同的風驅動液滴，Poelma 教授探討的液滴受到基版運動所驅動。在這樣的狀況下，以傳統的連續性流線方程來解釋，會在接觸線前沿遭遇奇異的問題。目前合理的解釋包含有滑移介面以及前導液膜。由於液膜的厚度僅數個奈米，且厚度的變化與分子間的凡得瓦力有關。使得相關液滴接觸角與液膜厚度的量測相當困難。Poelma 教授的團隊以整合型內反射搭配流體螢光的量測方法(TIRF, Total Internal Reflection Fluorescence)，來獲得液滴在固液氣三相線附近的液滴外型。研究中先顯示了有靜態液滴下 TIRF 與 AFM（原子力顯微鏡）的一致量測結果，但 AFM 的缺點在於無法獲得動態下的液滴前沿外型。其研究結果證實了前導液膜，是造成動態液滴前進的解釋。

由於筆者曾經就奈米尺度液滴在粗糙表面與具有電場的狀態下的外型進行研究，所以對 Hui Hu 教授以及 Poelma 教授的液滴動態研究特別有興趣。而分子動力模擬在此一介面現象上的研究，有其無法取代的優點。相信可以運用分子動力模擬的數值可視化方法，來探討與解釋若干開放問題。

在 26 日的專題演講中，來自日本 Toyohashi 科技大學的 IIDA 教授，介紹了以數值模擬與實驗量測所得到流場可視化成果，來比對流體運動所產生的噪音來源。其團隊特別針對新幹線列車的行進噪音與流場做量測，並且以風洞量測了噪音來源。研究顯示新幹線的單音噪聲(tonal noise)主要來自於集電弓在高速行駛下所生成的不穩定分離渦流對所造成。在此篇研究中，IIDA 教授指出音源量測與流場可視化，相互之間的比對，成為氣動力噪音

生成機制探討的重要工具。在未來的流場噪音壓制研究中，數值與音場計算模擬配合 PIV 的流場可視化技術，將可以大幅提昇音源的生成機制確認，進而採取有效的降噪措施。此一方面的研究，對於海軍的水下作戰有相當大的意義。由於水面下音源精確量測的困難性，搭配水槽模擬水動力與音源分佈狀況，配合數值分析所得到的流場相互比對，對於水下噪音的生成來源與產生機制應有相當大的探討空間。

來自韓國 Sungkyunkwan 大學的 H.S. KO 教授提出了以電腦斷層掃瞄的流場重建技術，來進行流場可視化以及流場控制。其團對以三部高速攝影機紀錄流場中目標粒子的速度，並運用斷層重建演算法來還原三維流場。對於複雜流場的可視化有相當深入的探討。

在 27 日的專題演講中，北京航天大學的 Feng Li-Hao 教授則回顧了流場遭遇鈍型物體時產生分離渦流對的主動式控制。特別是針對了其研究團對在 Plasma Actuator 以及 Synthetic Jet 兩種先進流場控制技術上的研究結果。Plasma Actuator, 電漿致動器為利用高電壓離子化氣體，在表面形成電漿。Synthetic Jet 主要是由震動薄膜、空腔以及噴嘴所組成。在薄膜的壓縮行程時吸入氣體至空腔，而在薄膜的膨脹行程時噴出環狀渦流。這兩種主動式的流場控制器安置在鈍型物體流場分離點的前方或後方，可以有效的降低分離渦捲的產生，也大幅降低了因渦捲而造成的震動。

會議結束後，於 6 月 30 日搭機返國，於 30 日下午返抵國門。

四、論文發表：

Effects of wettability on gas-water flow over the roughness nanochannels

Tsu-Hsu YEN

ABSTRACT: In the present study, molecular dynamics simulations are performed to explore the effects of wettability on gas-water flow over the roughness nanochannels. A "liquid-gas-vapor coexistence setup" is employed to maintain a constant thermodynamics state for individual equilibrium simulation and corresponded hydrodynamic case. Two control parameters are tuned, changing the properties of interest. (Ⅰ)To identify effects of interfacial gas density, the number of argon molecules is changed on initial setting. (Ⅱ)To simulate different wettability, the water-solid interaction energy is varied while the argon-solid interaction parameters are remained fixed. The fluid properties including hydrostatic and hydrodynamic states, such as potential energy (between water molecules and ambient particles), water and argon density contour and diffusion coefficients of argon molecules nearby the boundary regions are visualized and analyzed. The present simulation results reveal that the regions with lower potential energy have higher possibility for water molecules location and thus increase the momentum exchange. In addition, the argon diffusion coefficients adopt dramatic change nearby the roughened substrates after the external force added. The results also show the effective slip length are both significantly influenced by wall-fluid wettability and interfacial gas density.

Keywords: Wettability, Gas-Water Flow, Surface Roughness, Effective Slip Length

論文中文摘要：

潤濕性對含有介面氣泡之水流體在粗糙奈米流道中的影響

本研究採用分子動力模擬探討介面潤濕效應，對於氣體-水流體通過奈米尺度粗糙流道的影響。以矽晶格排列、水分子與氬分子分別代表了固體、流體與氣體分子材料。本研究採用了'流-氣-汽共存設定法'來保持每個算例具有相同的熱力條件（包含流靜與相對應的流動模擬）。研究中調變兩個控制參數以探討所欲比對的流體性質：(1)為探討汽體濃度對於介面行為的影響，研究中改變了介面間的氣體粒子數目；(2)調變流固交互作用強度以改變介面潤濕性，但汽體分子與固體間的參數則維持不變。本研究分析探討了流靜與流動性質。包含水分子與環境分子間的勢能分布、水與氣體的密度分布以及流體擴散係數等性質。模擬結果顯示了低勢能分布的位置上，水分子有較高的存在機率，並且因此增加了介面間的動量傳遞。此外，表面凹槽內的氬原子擴散係數受到外加力場的影響，產生了巨大的變化。結果也說明了有效滑移長度同時受到固液介面間潤濕性以及介面間氣體濃度的影響。

1 Introduction

Solid-fluid interfacial phenomena are getting much more attention in recent years. These mirco- or nano- scale unique interfacial properties come from high surface-to-volume ratio in microscopic systems in which the surface effects to be more important than in macroscopic systems. Some of important interfacial properties such as wettability and boundary slip are getting more important in many applications, e.g. membrane channels, soil science, filtration and bio- or neon-electro- mechanical-systems devices. Conventionally, two strategies of interfacial controlling have been provided: first is to alter the morphology of substrate's surface which can be considered as the physical mechanism and second is tuning the wall-fluid interaction parameters which is dictated by the material chemistry [1].

Recent experiments demonstrate that much higher slip length observed on smooth hydrophobic surfaces [2] or topological patterned substrates [3]. In the point view of molecular scale, the slip length influenced by many factors including surface morphology, surface lattice orientation [4], solid structure [5], and dissolved gas [6]. In addition, due to the liquid may slide on the gas film, the gaseous bubble is often considered as a central role of large slip [7]. Therefore, the influence of interfacial characteristics are closely related to the atomistic information and owning highly complicated relation [8].

Among the influential factors, the surface roughness and gas molecules are quite significant for interfacial phenomena. A roughened surface can be intentionally fabricated with elements mounted on or grooves indented in solid surfaces. Some previous molecular dynamic (MD) simulations dealt with the effects of surface obstacles or grooves in nanoscale flows [9, 10]. In their investigations, the micro- or nano-textured surfaces with grooves or cavities can produce micro- or nano-sized bubbles or a gas layer and act as a lubricant. By using the LBM, Hyväluoma and Harting [11] indicated that the air bubble results in the negative slip. They also found the slip length decreased with increasing shear rate. In nanoscale, due to the high surface tension of surrounding water, the gaseous structures will be dissolved or condensed to higher densities which make the gases behavior different. The physical mechanism of the nanobubble contained in nanochannel fluidic is somewhat different to the macro-scale scenario and is in need of further investigation.

The wettability can represent the static structure of equilibrium interfacial conditions of fluid in contact with a particular surface [10]. Huang et al. [12] investigated the slippage of water at various hydrophobic surfaces. They found the slip lengths on various surface can collapse onto a function of contact angle. Quere [3] indicated that the surface roughness and heterogeneous promote the effective slip length and the wettability. Priezjev et al. [13] have performed MD simulations of the flow past planar striped anisotropic substrates with mixed boundary conditions. However, the validity of the relationship between slippage and wettability for the nanoscale fluid with gas contained is worth further investigation. In this study, MD simulations were applied to investigate the liquid water over the groove-patterned substrate with and without entrapped gas molecules under various wettability setting. The fluid properties including hydrostatic and hydrodynamic states, such as effective slip length, density distribution, the diffusion coefficient and gas bubble menisci were compared and analyzed.

2 Methodology and simulation model

In this study, the hydrostatic wetting and Poiseuille flow phenomena on the roughened substrates are simulated. Various water-solid interaction energy with the same solid atomic arrangement, Si(100) substrate, are adopted to study the effect of wettability. We used the "liquid-vapor coexistence" procedure which is provided by Cao et al. [10] to maintain a constant thermodynamics state for individual simulation case in present simulations. The systems are built through the following procedures as shown in figure 1. As an initial condition, a sandwich-like cubic containing water molecules layers with a bottom layer of argon molecules are stacked in the middle of the channel. Then, we start to run our simulations to drive the system to reach a steady thermodynamic state. After the hydrostatic simulation finished, the middle section is segmented out only along the x direction to form a flow configuration. The Poiseuille flow system under consideration is composed of water and argon molecules confined between two parallel substrates with the same morphology and material of hydrostatic simulation cases. In present Poiseuille flow simulation, a constant external force stemming from the pressure gradient in the x direction is applied to the fluid particles. Due to the high thermal noise, a external force, $f_p = 0.02\sigma^3/\varepsilon$ corresponded to $2 \times 10^{12} \ m/\sec^2$, which is the same as previous simulation work [14] used so that fluid velocity profile could be retrieved with reasonable accuracy.

Data sampling is carried out at a period of 300τ to 1100τ, which corresponds to 0.5 to 1.83nsec. In present argon-water coexistence simulations, the calculated systems contain about 7000~8500 water molecules. In the Poiseuille flow simulation, the systems have about 4000~5500 water molecules. There are two computational

domains divided into a number of bins which one is $\Delta x \times \Delta y \times \Delta z = 0.2\sigma \times L_y \times 0.2\sigma$ for two dimensional contours and another one is $\Delta x \times \Delta y \times \Delta z = L_x \times L_y \times 0.2\sigma$ for one dimensional profiles.
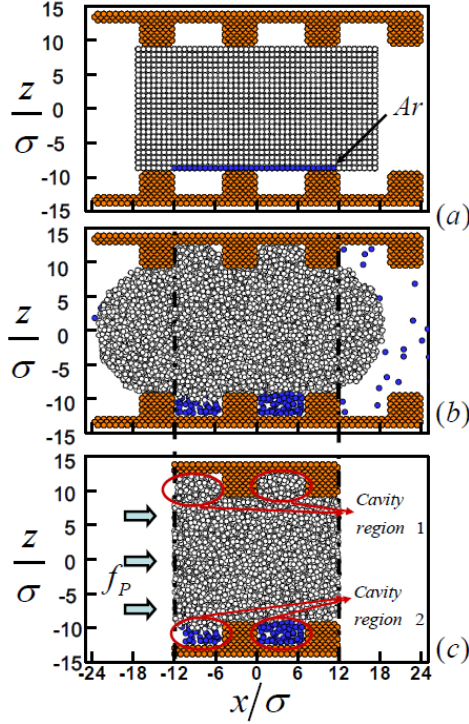

Fig. 1 The simulation system and its constructing procedures. The simulation systems are constructed through three stage: (a) initial setup stage, (b) hydrostatic simulation stage: argon-water-vapor coexistence in the nanochannel, and (c) hydrodynamic simulation stage: channel Poiseuille flow.

In the case of the Poiseuille flow of a Newtonian fluid under constant external force, the macroscopic hydrodynamics gives a parabolic profile. We sampled the averages of the velocity profiles covering the fluid channel and grooves. The effective slip length L_s, as a measure of fluid slippage, is defined in Navier slip formula $L_s = u_s/(du_x/dz)$ where u_s and du_x/dz, respectively are the slip velocity and the velocity gradient in the normal direction on the wall-fluid baseline. The effective slip length is obtained by second order polynomial fit of the velocity but, to avoid the non-Newtonian effect, with the data in near-wall region containing argon bubble excluded.

The simulation model system consists of water, argon molecules and solid atoms. The solid boundary lies on the xy-plane, where periodic boundary conditions are posed in both the x- and y-directions. The TIP4P model [15] is employed for water molecules simulation. The cut-off distance of $r_c = 4.0\sigma$ was adopted for the Lennard-Jones (LJ) and Coulomb interaction. The cut-off distance was applied with reference to the Oxygen sites. The LJ and Coulomb interaction potentials employed in the present simulations are both truncated and shifted. The 12-6 LJ potential is taken to measure the interaction between two oxygen atoms and between oxygen and solid atoms. The Coulomb potential is applied to evaluate the interaction between charges. The parameter r is the separation distance between the interacting molecules/ atoms, ε is an energy scale characterizing the strength of the interaction, and σ denotes a molecular length scale. Conventionally, σ for length, ε for energy, $\tau = (m\sigma^2/\varepsilon)^{1/2}$ for time, and ε/k_BT for temperature are used as the reduced units in MD simulations. For water, $e = 4.803 \times 10^{-10} esu$, $\sigma \equiv \sigma_{OO} = 3.154$ Å, $\varepsilon = 0.155$ kcal/mole and $\tau = 1.66 \times 10^{-12}$ sec. Hereafter, the physical properties are presented based on the reduced units addressed above. The charges and Lennard-Jones parameters are taken from reference [6] and are summarized in table 1. Newton's equations of particle motion are solved by using predictor-corrector algorithm with time step $5 \times 10^{-4}\tau$. In both hydrostatic and hydrodynamic simulation, the system temperature is set at 150K and unchanged until 5000 time-steps initially. Then, the temperature is raised to 300K at the 10,000th time-step and then maintained at 300K. The Nośe-Hoover thermostat is employed for water molecules temperature control in

only *y* direction.

Table 1: Charges and Lennard-Jones parameters adopted in the present simulations

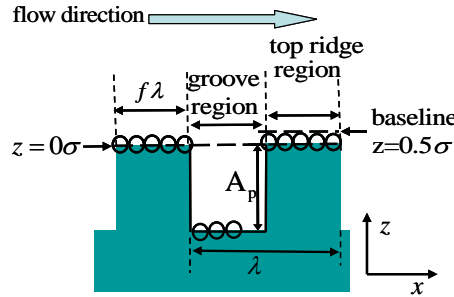| Ion/molecule	$q_i(e)$	$\sigma_{\alpha\beta}/\sigma\,,\sigma=\sigma_{oo}$	$\varepsilon_{\alpha\beta}/\varepsilon\,,\varepsilon\equiv\varepsilon_{oo}$
O $\leftrightarrow$ O (H$_2$O)	-1.04	$\sigma_{oo}=0.3154nm$	$\varepsilon_{oo}=0.155kal/mole$
H $\leftrightarrow$ H (H$_2$O)	0.52	0	0
Wall $\leftrightarrow$ H$_2$O		$\sigma_{Si-O}/\sigma=1.0315$	$\varepsilon_{Si-O}/\varepsilon=0.4/0.8/1.2/1.6/2.0$
Ar $\leftrightarrow$ Ar		$\sigma_{Ar-Ar}/\sigma=1.0812$	$\varepsilon_{Ar-Ar}/\varepsilon=1.538$
Ar $\leftrightarrow$ H$_2$O		$\sigma_{Ar-O}/\sigma=1.045$	$\varepsilon_{Ar-O}/\varepsilon=1.242$
Wall(Si) $\leftrightarrow$ Ar		$\sigma_{Si-Ar}/\sigma=1.132$	$\varepsilon_{Si-Ar}/\varepsilon=0.81$

Fig. 2 Schematic illustration of a substrate with grooved patterns. A_p denotes the groove height, λ the grooved pattern period and $f\lambda$ the spacing between two grooves where f is the surface fraction.

Figure 2 defines the period (λ) and amplitude (A_p) of the groove. In static simulations, the substrate dimensions of computational domain in the *x, y* and z directions are $L_x \times L_y \times L_z = 48\sigma \times 12\sigma \times 19\sigma$, whereas in hydrodynamic simulations, the dimensions of the fluid computational domain in the *x, y* and *z* directions are $L_x \times L_y \times L_z = 24\sigma \times 12\sigma \times 19\sigma$ (L_z denotes the distance between two baselines of substrate). In present study, the parameters of periodic patterned substrate are set as: amplitude $A_p = 3.48\sigma$, surface friction $f = 0.4$ and period $\lambda = 12\sigma$. In order to reduce the computational expense, the solid atoms are fixed at their respective positions. The potential energy is calculated in each bin as: $u_{bin}(r_{ij}^{bin}) = 4\varepsilon\left[(\sigma/r_{ij}^{bin})^{12} - (\sigma/r_{ij}^{bin})^6\right]$, where r_{ij}^{bin} is the distance between the *i*th water molecule (located inside the bin) and the *j*th ambient particle including argon and solid atom (located both inside and outside the bin).

The Einstein expression of diffusion coefficient can be written as: $D_{Ar}(\tau) = \lim_{\tau\to\infty}\frac{1}{6N_a t}\left\langle\sum_{j=1}^{N_a}\left[r_j(\tau) - r_j(0)\right]^2\right\rangle$.

Although this relation is derived from equilibrium system, it can used for non-equilibrium system as well. The previous study [16] denoted that diffusivity in Couette flow is indistinguishable from the results of equilibrium simulations. In present study, the translational diffusion is measured base on the water molecule's center-of-mass coordinates.

3 Results and Discussion

A series of MD simulations of solid-argon-water systems is performed to investigate the effect of the argon interfacial density and wettability. The different argon concentrations are set in initial conditions to perform the

comparison between the results of different interfacial argon densities. The interfacial density of argon molecules on the solid-fluid interface is defined as: $\rho_{s,Ar}\sigma^2 \equiv N_{Ar}/S$, where N_{Ar} is the number of argon nearby the particular substrate and S is the project area of this surface. Hereafter, some characteristic properties nearby the wall-fluid interface including water and argon properties and slip length are simulated and discussed in following segments. Two boundary states i.e., with and without interfacial gas molecules are simulated and compared. Thus, the effect of interfacial gas and wettability can be analyzed.

3.1 Interfacial Water Properties

In this section, we focus the interfacial water properties such as fluid number density, potential energy of ambient particles (solid atoms) to water molecules, diffusion coefficient and rotational diffusion coefficient inside the grooves of roughened substrates.

Water properties nearby the interface without argon molecule Two models, Cassie and Wenzel, are adopted to describe the degree of wettability on roughness surface. In the Cassie model, the roughness cavities are assumed to have little liquid in it, while in the Wenzel model, the cavities is assumed to be of sufficiently high liquid density. However, the separate line between these two states is far from distinct in nanoscale. Rasaiah et al. [17] indicated that the water molecules exhibit different properties inside the nanoscale cavities. These different properties include water filled and empty coexistence states and highly sensitivity of perturbation. In present study, some unique phenomena such as discontinue epitaxial layering distribution and lower water density on central cavity's region are observed (shown as figure 3a). These properties may induce the inadequacy of Cassie and Wenzel models in nanoscale.

Figure 3 shows the wall-fluid interfacial water density and corresponded potential energy for various parameters of water-solid interaction energy in Poiseuille flow. As shown in figure 3a, following the increasing of wall-fluid interaction energy, the space inside the grooves fills with water molecules progressively. And therefore, the epitaxial layering distributions inside the cavities are enhanced. The up most plot of figure 3a shows the water density nearby the substrate for $\varepsilon_{wf}/\varepsilon_{ff}=0.4$. The water density inside the grooves is obviously lower in this plot. It can be inferred that, in the case of lower water-solid interfacial energy, the boundary condition is more likely proposition of the Cassie state. On the other hand, in the case of larger interfacial energy, i.e. $\varepsilon_{wf}/\varepsilon_{ff}=2.0$, the Wenzel model is more appropriate to describe the interfacial condition. The obviously epitaxial layering distribution enhances the wall-fluid momentum exchange and thus increases the hydrophilicity and induces the no slip condition or even interfacial multi-layer sticky phenomena. Due to the moderate water density and layering distribution, in the intermediate regime of $\varepsilon_{wf}/\varepsilon_{ff}$ e.g., 0.8~1.2, the boundary conditions can be considered transferred between Wenzel and Cassie states.
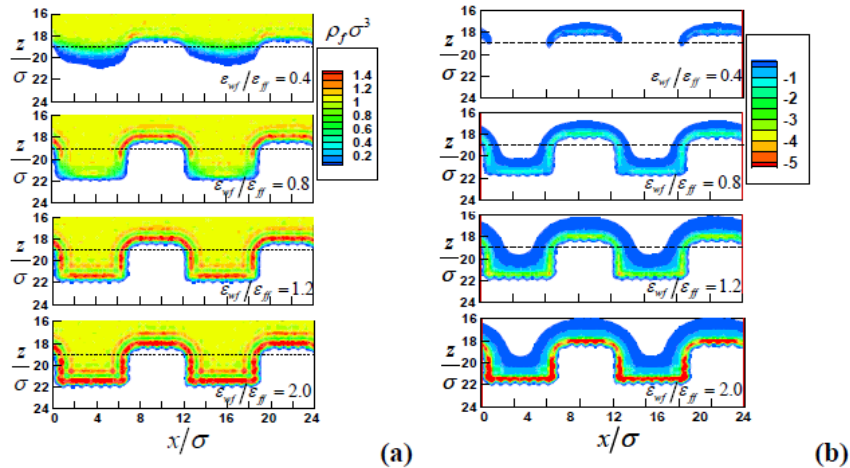

Fig. 3 (a) the number density contours and (b) potential energy contours of water nearby the upper boundary for water-solid interaction energy $\varepsilon_{wf}/\varepsilon_{ff}=0.4$, 0.8, 1.2 and 2.0, from top to down respectively. The dotted lines denote the position of inner most layers of substrate particles.

Figure 3b indicates that water molecules tend to localized in low potential regions inside the grooves. When the

wall-fluid interface is more hydrophobic (e.g., $\varepsilon_{wf}/\varepsilon_{ff}$ =0.4), there is almost no low potential regions inside the grooves observed on upper most plot of figure 3. This phenomenon refers to the water-vapor interface exist on the groove regions and also confirms that the Cassie state can represent this boundary state. On the other hand, for the case of $\varepsilon_{wf}/\varepsilon_{ff}$ =2.0, i.e., the most hydrophilic boundary in out simulation, an obviously low potential layer occurs along the wall inside the grooves. The distribution of this low potential layer corresponds to the position of first layer of density contour and can be considered the reason of high density value of first layering. It indicates that more fluid particles may accumulate on the region with lower potential energy. Consequently, the second and third density layering distributions can be attributed to the result of fluid first layering. However, for the $\varepsilon_{wf}/\varepsilon_{ff}$ =1.2 case, the lowest regions of potential distribution are located on the corners of groove's bottom which are different to the location of highest density layering region. This localizing inconsistent may attribute to the interaction of two directional density layering distributions.

Water properties nearby the interface with argon molecules   Comparing with figure 3, the figure 4 demonstrates the similar contours (water density and potential energy) but with interfacial argon molecules. The water particles are observed almost unoccupied in the space of groove bottom region due to the argon molecules existence. The water density layering is vanished inside the cavities thus reduces the solid-water momentum exchange. The potential energy contours (shown as figure 4b) demonstrate the effect of the parameter $\varepsilon_{wf}/\varepsilon_{ff}$.

The variations of potential energy are obviously enhanced with the parameter $\varepsilon_{wf}/\varepsilon_{ff}$ increasing on solid top ridge while much minor influence occurred on groove regions. From the view point of momentum exchange, the comparison of potential energy contours between 3b and 4b indicate that the effects of interfacial gas molecules are different depending on the wettability. In the case of low $\varepsilon_{wf}/\varepsilon_{ff}$ (i.e., $\varepsilon_{wf}/\varepsilon_{ff}=0.4$), the existence of interfacial gas molecule enhances the solid-water momentum exchange in which the water-vapor interfaces exist on the groove regions. On the other hand, when the water molecules occupy the cavities space (i.e., $\varepsilon_{wf}/\varepsilon_{ff}>0.4$), the effect of interfacial argon decreases the momentum exchange between water and ambient particles.
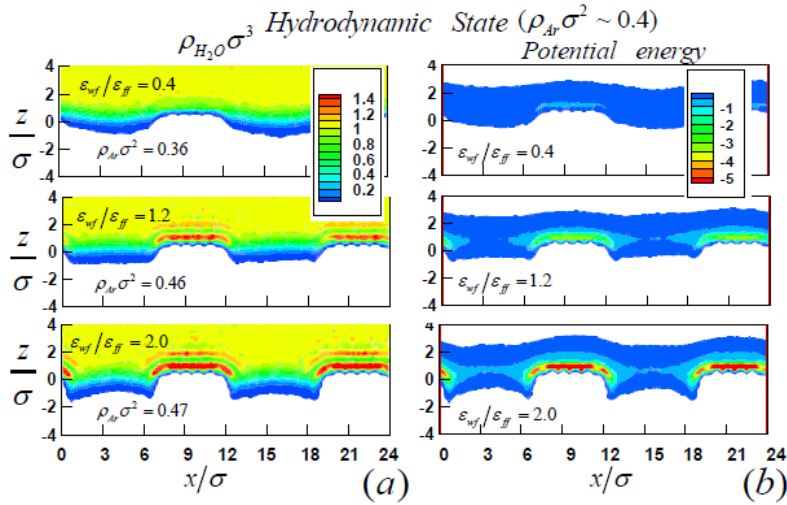

Fig. 4 (a) Number densities contours of water nearby the bottom boundaries and (b) Potential energy contours for corresponded cases. From top to down, the wall-water interaction energies are increased as $\varepsilon_{wf}/\varepsilon_{ff}$ = 0.4, 1.2 and 2.0.

3.2 Interfacial Argon Properties

The figure 5 reveals the argon densities difference between equilibrium hydrostatic state and non-equilibrium Poiseuille flow state. The plots from top to down represent the results of wall-water interaction energies with $\varepsilon_{wf}/\varepsilon_{ff}$ =0.4, 1.2 and 2.0, respectively. The argon density layering emerges from the edges of the grooves. These argon density layering phenomena are more enhanced with the solid-water interaction energy increased

especially on the corners of groove bottom. The high density of gaseous structure can be inferred from the high surface tension of the surrounding water at the nanoscale. The higher $\varepsilon_{wf}/\varepsilon_{ff}$ tends to promote the water surface tension and thus increases the argon density inside the grooves. The hydrodynamic effect reduces the argon density inside the cavities especially in the cases of lower solid-water interaction energy due to some water molecules invade into the cavities via external force field. Although argon-solid interaction parameters remained fixed, the variation of wettability induces distinct different argon morphologies inside the grooves both in hydrostatic and hydrodynamic states. The morphologies of argon molecules accumulated inside the groove form as a convex shape for higher $\varepsilon_{wf}/\varepsilon_{ff}$ cases while own a shallow concave shape for lower $\varepsilon_{wf}/\varepsilon_{ff}$ cases. These phenomena are more pounced in hydrodynamic state. Two reasons of this phenomenon can be attributed to following two reasons: one is hydrodynamic effect decreasing the argon density; another one is the higher solid-water interaction energy resulting in more hydrophilic grooves, thereby inducing more water molecules into grooves along the side walls via an external force field.

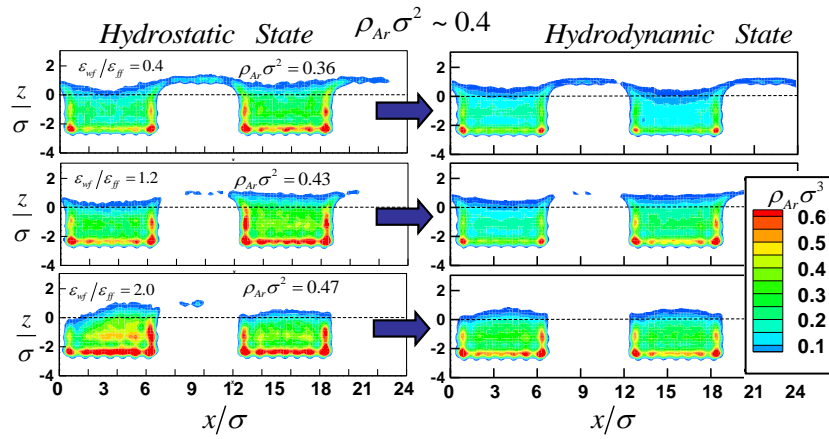Fig. 5 The number density contours of argon nearby the bottom boundary before and after external force fields added. From top to down, the plots show the results of wall-water interaction energies with $\varepsilon_{wf}/\varepsilon_{ff} = 0.4$, 1.2 and 2.0.
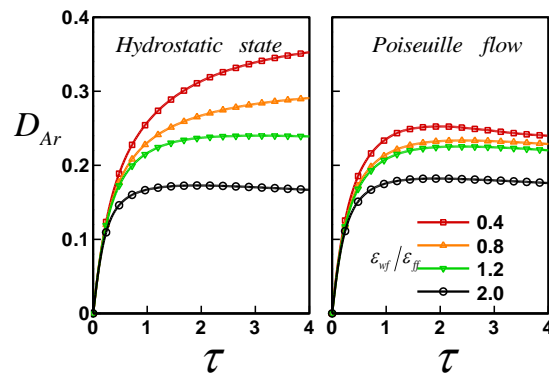

Fig. 6 Diffusion coefficient measurements for argon molecules inside the cavities before (left plot) and after (right plot) the external force fields added

13

Figure 6 demonstrates the diffusion coefficient of argon molecules inside the groove regions for (a) hydrostatic state and (b) hydrodynamic state. These argon diffusion coefficient profiles indicate that the argon mobility increased with the wattability decreasing. Although the hydrodynamic effect tends to reduce the argon density inside the groove, this hydrodynamic effect also dramatically reduce the argon mobility except the case of $\varepsilon_{wf}/\varepsilon_{ff} = 2.0$. This result can be attributed to some water molecules flow into the grooves and restrict the movement of argon particles. The low mobility of argon molecules indicates that even on highly hydrophobic substrate, the argon bubbles inside the groove can no longer be considered as gaseous structure in hydrodynamic state. The results also indicate that both wettability and hydrodynamic effects can obviously alter the mobility of interfacial gas molecules.

3.3 Slip length influenced by wettability and surface argon density

Figure 7 demonstrates the slip length as a function of water-solid interaction energy, $\varepsilon_{wf}/\varepsilon_{ff}$ in the cases without and with various interfacial argon densities. With the situation of no interfacial gas density, the boundary slip is enhanced by decreasing wettability when $\varepsilon_{wf}/\varepsilon_{ff}$ was below 1.2. With higher water-solid interaction energy and in turn, the boundary more like Wenzel state, flow through the nanochannel may encounter the protruding elements of rough surface and result in low slip length. On the other hand, further reducing $\varepsilon_{wf}/\varepsilon_{ff}$ can induce the boundary transition from Wenzel to Cassie state. This state transformation alters the water-solid interface into water-vapor interface, reduces the flow disturbing by the roughness features and thus promotes the slip length.

The effects of flowing water containing interfacial gas molecules on slip length are shown as filled symbols of figure 7. In cases of high wall-fluid interaction energy ($\varepsilon_{wf}/\varepsilon_{ff} > 1.2$), higher interfacial argon density $\rho_{Ar}\sigma^2$ means larger argon bubbles with convex shape. Poiseuille flow through the boundary may result in an increase in the low friction area and encountering larger protruding bubbles. Further increasing the interfacial argon density will not promote the boundary slip length. For the lower wall-fluid interaction energy conditions ($\varepsilon_{wf}/\varepsilon_{ff} < 1.2$), the morphologies of argon molecules accumulated near the boundary can be consider as shallow concave shape on groove region and combined with gas films on top ridge region (shown as figure 5a). Further increasing the interfacial argon density will dramatically enhance the boundary slip.
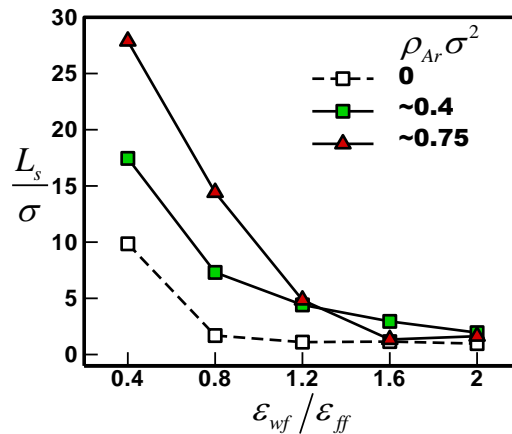

Fig. 7 The slip length as a function of the wall-water interaction energy for various interfacial argon densities

14

4 Concluding remarks

In the present study, both equilibrium and non-equilibrium molecular dynamics simulations are performed to explore the effects of wettability on gas-water flow over the roughness nanochannels. A "liquid-gas-vapor coexistence setup" is employed to maintain a constant thermodynamics state for individual equilibrium simulation and corresponded hydrodynamic case. Two control parameters, interfacial argon density and water-solid interaction energy, are tuned to identify the effects of interfacial gas and wettability while the argon-solid interaction parameters are remained fixed. The fluid properties, such as potential energy (between water molecules and ambient particles), water and argon density contour, local diffusion coefficients nearby the boundary regions and effective slip length are visualized and analyzed.

Based on the present MD simulations, the physical finding can be summarized as follows:

1. Following the increasing of $\varepsilon_{wf}/\varepsilon_{ff}$, the space inside the grooves fills with water molecules progressively. And therefore, the epitaxial layering distributions inside the cavities are also enhanced. In the case of lower $\varepsilon_{wf}/\varepsilon_{ff}$, the boundary condition is more likely Cassie state while the boundary condition with larger $\varepsilon_{wf}/\varepsilon_{ff}$ is more appropriate to Wenzel state. The boundary conditions can be considered transferred between Wenzel and Cassie states when the water-solid interaction energy set as intermediate regime e.g., $\varepsilon_{wf}/\varepsilon_{ff}$ =0.8~1.2. Furthermore, the distribution of low potential layer corresponds to the position of first layer of density contour and can be considered the reason of high density value of first layering.

2. Although the hydrodynamic effect tends to reduce the argon density inside the groove, this effect also dramatically reduce the argon mobility except the case of $\varepsilon_{wf}/\varepsilon_{ff}=2.0$. This result can be attributed to some water molecules flow into the grooves and restrict the movement of argon particles. The low mobility of argon molecules indicates that even on highly hydrophobic substrate, the argon bubbles inside the groove can no longer be considered as gaseous structure in hydrodynamic state.

3. The effects of flowing water containing interfacial gas molecules on slip length can be considered as following two aspects. In cases of higher wall-fluid interaction energy ($\varepsilon_{wf}/\varepsilon_{ff}$ >1.2), more interfacial argon density may result in an increase in the low friction area and encountering larger protruding bubbles. Further increasing the interfacial argon density will not promote the boundary slip length. For the lower wall-fluid interaction energy conditions ($\varepsilon_{wf}/\varepsilon_{ff}$ <1.2), the morphologies of argon bubble can be consider as shallow concave shape on groove region and combined with gas films on top ridge region. Further increasing the interfacial argon density will enhance the boundary slip.

References

1. Tretyakov N and Müller M. Correlation between surface topography and slippage: a Molecular Dynamics study. *Soft Matter,* Vol. 9, pp 3613-3623, 2013.

2. Zhu Y and Granick, S. Rate-dependent slip of Newtonian liquid at smooth surfaces. *Phys. Rev. Lett.,* Vol. 87, No. 9, pp 096105, 2001.

3. Quéré D. Wetting and roughness. *Annu. Rev. Mater Res.,* Vol. 38, pp. 71-99, 2008.

4. Soong C Y, Yen, T H and Tzeng P Y. Molecular dynamics simulation of nanochannel flows with effects of wall lattice-fluid interactions. *Phys. Rev. E,* Vol. 76, No. 3, pp. 036303, 2007.

5. Ho T A, Papavassiliou D V , Lee   L L   and Striolo A. Liquid water can slip on a hydrophilic surface. *Proc. Natl. Acad. Sci.,* Vol. 108, No.39, pp. 16170-16175, 2011.

6. Sendner C, Horinek D, Bocquet L and Netz R R. Interfacial water at hydrophobic and hydrophilic surfaces: Slip, viscosity, and diffusion. *Langmuir*, Vol. 25, No. 18, pp. 10768-10781, 2009.

7. Hyväluoma J, Kunert C and Harting J. Simulations of slip flow on nanobubble-laden surfaces. *J. Phys.: Cond. Matter,*Vol. 23(18), pp. 184106, 2011.

8. Lauga E, Brenner M P and Stone H A. Microfluidics: the no-slip boundary condition. In Tropea C, Yarin A L and Foss J F. Eds., *Experimental Fluid Dynamics*, New York: Springer, Ch15, 2005.

9. Cottin-Bizonne C, Barrat J L, Bocquet L and Charlaix E. Low-friction flows of liquid at nanopatterned interfaces. *Nature material,* Vol. 2, No. 4, pp. 237-240, 2003.

10. Cao B Y, Chen M and Guo Z Y. Liquid flow in surface-nanostructured channels studied by molecular dynamics simulation. *Phys. Rev. E*, Vol. 74, pp. 066311, 2006.

11. Hyväluoma J and Harting J. Slip flow over structured surfaces with entrapped microbubbles. *Phys. Rev. Lett.,*Vol. 100, pp. 246001, 2008.

12. Huang D.M., Sender C., Horinek D., Netz R.R. and Bocquet L., "Water slippage versus contact angle: a quasiuniversal relationslip," *Phys. Rev. Lett.*, Vol. 101, pp. 226101, 2008.

13. Priezjev N V, Darhuber A A and Troian S M. Slip behavior in liquid films on surfaces of patterned wettability: Comparison between continuum and molecular dynamics simulations. *Phys. Rev. E,* Vol. 71, No. 4, pp. 041608, 2005.

14. Joseph S and Aluru N R Why are carbon nanotubes fast transporters of water? *Nano Lett.,* Vol. 8, No. 2, pp.452-458, 2008.

15. Rapaport D C. *The art of molecular* dynamics *simulation,* Cambridge university press, 2004.

16. Bitsanis I, Magda J J, Tirrell M and Davis H T. Molecular dynamics of flow in micropores. *The J. Chem. Phys.*, Vol. 87, pp.1733, 1987.

17. Rasaiah J C, Garde S and Hummer G. Water in Nonpolar confinement: from nanotubes to proteins and beyond. *Annu. Rev. Phys. Chem*., Vol. 59, pp. 713-40, 2008.

五、建議事項：

　　國際流場可視化論壇（ISFV）每兩年舉辦一次，此次為第 15 屆。研討內容偏重流場可視化、量測、相關數據資料的成相技術以及現象觀察與物理機制探討。本次大會邀請了各國頂尖之研究學者提出專題報告，參加的論文超過三百篇。

　　筆者參加此次會議，除了有機會與流體研究領域的頂尖學者就近討論，更可以瞭解微奈米流場研究的大方向。

　　而個人的另一個感想，則是與會學者所提出的問題，多為先進技術的理論問題。這顯示了尖端技術的發展，還是要有透澈的理論基礎。如何尊重專業，建立專業，培養出能夠真正分析問題、尋求根本解決之道的海軍軍官，這或許是我們必須反思的課題。

　　此次個人參加此國際學術研討會，受益良多，建議可多鼓勵本校教師多爭取國科會的研究經費，利用寒暑期赴國外研習，吸收新知，並將其應用於教學內容。

附錄：活動照片

本人與徐子圭副教授在會場合影

本人於 15th ISFV 研討會發表論文

The 16th International Symposium on Flow Visualization (ISFV16)

Jun. 25 (Wed.)

A1   Jun. 25 (Wed.), 10:00 - 10:50, A1   Plenary lecture-1

Chair: Jean Pierre Prenel (French Optical Society)

ISFV16-1136	Quantitative Visualization of Complex Thermal Fluid Phenomena by using Advanced Flow Diagnostic Techniques
	Hui Hu (Iowa State University, United States)

Jun. 25 (Wed.), 11:00 - 12:40, A1   Track01-1. PIV/PTV-1

Chair: Dirk Michaelis (LaVision GmbH, Germany)

ISFV16-1276	Toward the Development of the Single Camera Three-Dimensional PTV by using a Doppler-Phase-Shifting Holography
	Nao Ninomiya, Yamato Kubo, Daisuke Barada, Tomohiro Kiire (Utsunomiya University, Japan)
ISFV16-1261	Particle depth detection based on a novel technique of phase-shifting digital holography
	Kazuo Ohmi (Osaka Sangyo University, Japan), Chuan-qi Cao, Sudat Tuladhar (Graduate School of Osaka Sangyo University, Japan)
ISFV16-1244	Reconstruction of volumetric particle field from a light field image
	Syo Ogawa, Tatsuya Kawaguchi, Isao Satoh, Takushi Saito (Tokyo Institute of Technology, Japan)
ISFV16-1078	Research on three-dimensional PIV system with Plenoptic lens
	Chiharu Fujimori, Yoshisada Ohashi, Koh Ikeda (Ibaraki National College of Technology, Japan)
ISFV16-1098	The Research of Particle Image Velocimetry Based on Optical Flow
	Zhan Huang, Hong wei Wang, Yu Ma (China Academy of Aerospace Aerodynamics, China)

Jun. 25 (Wed.), 14:00 - 14:40, A1   Keynote lecture-1

Chair: Roesgen Thomas (ETH, Switzerland)

ISFV16-1334	Moving droplets -- the measurement of contact lines
	Christian Poelma (Delft University of Technology, Netherlands), J. Westerweel (TU Delft , Netherlands)

Jun. 25 (Wed.), 14:50 - 15:10, A1   Asanuma Award. Asanuma Award

ISFV16-1341	Taming Droplets by Visualization
	Kyung chun Kim (Pusan National University, Korea)

Jun. 25 (Wed.), 15:10 - 15:30, A1   DaVinci Award. DaVinci Award

ISFV16-1342	Five Centuries of Speckle Photography: from Da Vinci to Nowadays
	Nikita A Fomin (Luikov Heat and Mass Transfer Institute, Belarus)

Jun. 25 (Wed.), 15:40 - 17:40, A1   Track02-1. Micro and Nano-fluidics, Micro-gravity Flows

Chair: Han seo Ko (Sungkyunkwan University, Korea)

ISFV16-1003	Effects of wettability on gas-water flow over the roughness nanochannels
	Tsu-hsu Yen (R. O. C. Naval Academy, Taiwan)
ISFV16-1232	Multiscale modeling and simulation of biomolecule diffusion on the reaction field in micro bioanalysis device
	Yuma Suzuki, Tetsuhide Shimizu, Ming Yang (Tokyo Metropolitan University, Japan)
ISFV16-1171	VISUALIZATION OF THERMAL FLOW IN ASYMMETRIC MICRO PULSATING HEAT PIPES
	Jaeyong Sung, Young bae Kim, Myeong ho Lee (Seoul National University of Science andTechnology, Korea)
ISFV16-1146	flow visualization around flame on condensed fuels in low gravity environment
	Hiroki Abe, Akihiko Ito (Hirosaki University, Japan)
ISFV16-1297	Visualization and Measurement of the Self-propelled Motion of Janus Micro-particles
	Xu Zheng, Zhanhua Silber-Li (Institute of Mechanics, Chinese Academy of Sciences, China)
ISFV16-1203	Fluidic watering device applied to agriculture
	Yasuki Nakayama (Future Technology Research Institute, Japan), Takashi Tanaka (Yasuhisa KOKI Co.,Ltd, Japan)

A2   Jun. 25 (Wed.), 11:00 - 12:20, A2   Track04-1. Heat and Mass Transfer-1

Chair: Kenneth Kihm (The University of Tennessee, United States)

ISFV16-1083	Heat transfer and Flow Characteristics of One and Double rows of Impinging Circular Jets
	Kouichirou Yogi (University of the Ryukyus, Japan)
ISFV16-1177	Impinging jet as a method for enhancement of rectification effects in hybrid synthetic jet actuator
	Jozef Kordik, Zuzana Broukova, Zdenek Travnicek (Institute of Thermomechanics, Czech Republic)

大會議程截錄